JOURNAL OF MATERIALS SCIENCE 28 (1993) 2049–2060

Effect of microstructure on elevated-temperature fracture behaviour of two-dimensional carbon/carbon composites

S. SENET, R. E. GRIMES, K. W. WHITE
College of Engineering, University of Houston, Houston, TX 77204, USA
D. L. HUNN
LTV Missiles and Electronics Group, Dallas, TX, USA

The fracture behaviour of two-dimensional carbon/carbon composites has been studied at temperatures upto 1650 °C, using both chevron-and straight-notch single-edge notch beam (SENB) specimens. In all cases, the *R*-curve behaviour and fracture toughness variations with specimen orientation and temperature are characterized and correlated with the specific microstructure and failure micromechanisms. Higher crack growth resistance and fracture toughness of the longer fibre composite are attributed to the enhanced fibre pull-out and fibre bridging in the following wake region. The relative contribution from the frontal and following wake zone is determined experimentally by the use of renotching methods which demonstrate the effectiveness of the traction zone behind the crack tip. The temperature effects on the toughening mechanisms are examined in terms of crystal structure and fibre matrix interfacial characteristics.

1. Introduction

Carbon-matrix-reinforced carbon-fibre composites have found promise in numerous aerospace applications over the last two decades. Their low density and excellent refractory properties make them prime candidates for severe high-temperature environment applications [1]. Considerable research and development efforts are presently directed towards carbon/carbon composites as high-performance structural members to exploit their unequalled high-temperature strength and stiffness properties [2]. Although strength properties of these composites have been well documented over a broad range of temperatures, a thorough characterization of their fracture behaviour in the vicinity of the anticipated service temperatures remains noticeably absent from the literature.

This study will provide the groundwork for a fundamental understanding of the micromechanical failure events involved in the complex fracture process of these carbon/carbon composites. The fracture response of two different fibre architectures will be studied at temperatures up to 1650 °C. One composite, reinforced with a carbon fibre felt, will be compared with a highly structured woven architecture of continuous fibres. The behaviour differences of these related, yet distinctly unique two-dimensional composites, will not only demonstrate the effect of fibre length, and contrast the highly ordered, woven fibre architecture to that of the more economical chopped fibre structure, but also address the critical role of the matrix.

The plane strain fracture toughness, K_{IC}, and the crack growth resistance curves (*R*-curves) will be used here to characterize the fracture behaviour. The fracture toughness parameter serves as a useful design guideline for evaluating brittle materials under the restrictions of linear elastic fracture mechanics (LEFM) assumptions, where critical loading and geometry conditions predict crack instability [3]. *R*-curves provide the basis for stable crack growth behaviour studies in these highly nonlinear materials. The changes in crack growth resistance with crack length represent the toughening increment induced by the microstructure as the crack extends. Renotch experiments separate this microstructural contribution to toughening into two sources, that from the frontal process zone, and that from the following wake region. These experimental observations are then correlated with fractographic and internal structure studies to examine the micromechanical failure processes characteristic of these two carbon/carbon composites.

2. Experimental procedure

2.1. Materials

The two-dimensional discontinuous fibre carbon/carbon material used for this research was developed for use in aircraft brake components. It consists of a non-woven, high-density carbon felt, impregnated in a multi-step process. The first infiltration is with a thermosetting resin precursor. The second is with a pitch precursor, utilizing a high-pressure impregnation

0022–2461

TABLE I Physical and mechanical properties of the two carbon/carbon composites

		Kobe C/C (discontinuous fibres)	ACC 4 (continuous fibres)
Bulk Density (g cm^{-3})		1.54	1.68
Porosity (%)		16	6
Fibre volume fraction (%)		40	55
Compressive strength	0°	200	180
(MPa)	90°	130	180
Flexural modulus	L–T	45	60
(GPa)	L–S	40	45
Room temperature	L–T	10.4	22.7
toughness	T–L	8.0	22.7
(chevron-notch	L–S	7.5	19.8
specimens)			
(MPa m$^{1/2}$)	T–S	6.8	19.8

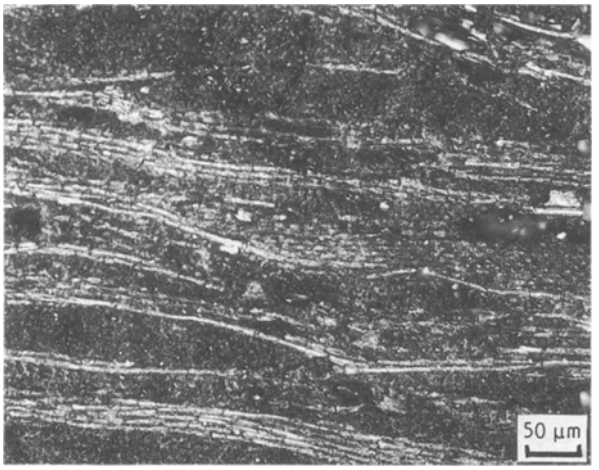

Figure 1 Optical micrograph of the discontinuous fibre carbon/carbon composite. View of the LS surface.

technique. Further details concerning the material production techniques are not available. The 6–7 μm diameter T-300 fibres are pyrolysed from a polyacrylonitrile (PAN) precursor. The bulk density was determined to be 1.54 g cm^{-3}, with a total porosity of 16% (see Table I). The optical micrograph of Fig. 1 typifies the resulting near-planar structure of this composite.

The two-dimensional woven continuous fibre carbon/carbon composite studied here, is also a state-of-the-art structural material designated Advanced Carbon/Carbon (ACC-4). ACC-4 also incorporates PAN-based T-300 fibres, woven into an eight harness satin fabric; however, the matrix is derived from multiple impregnations with K-640 phenolic resin. The three major processing steps are layup and cure, pyrolysis, and densification. The bulk density was found to be 1.68 g cm^{-3}. The optical micrograph of Fig. 2 characterizes the woven, laminar nature of this composite.

2.2. Specimen configuration

Bend-bar-type specimens were used for all the subject fracture experiments. The bend bar lengths were selected to accommodate a 60 mm test span. A span-to-width ratio (S/W) range of 5–8 was maintained to satisfy beam bending considerations, where S is the test span. The specimen width, W, and thickness, B, were held nominally equal to 10 mm. Accepted ranges of B fall between 0.25 W and 1.0W [4]. Both straight-notch and chevron-notch style bend bars were manufactured and tested for the two composites included in this research (Fig. 3). The specimen notches were machined using 0.25 mm thick, 100 mm diameter diamond-impregnated saw blades.

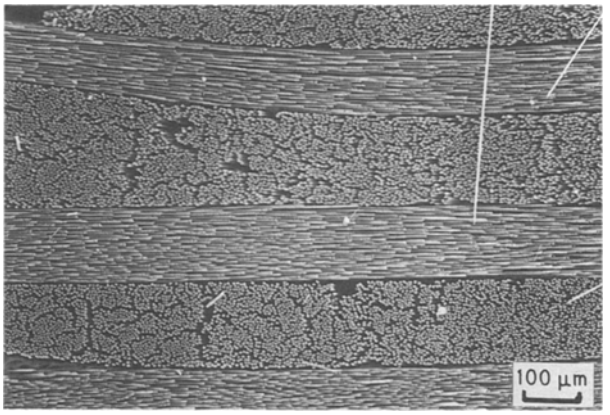

Figure 2 Optical micrograph of the continuous fibre carbon/carbon composite. View of the LS surface.

2.3. Specimen orientations

Both of these two-dimensionally reinforced composite materials are expected to be highly anisotropic. Accordingly, the formalism adopted, as shown in Fig. 4, arbitrarily assigns a longitudinal (L) direction to one edge of the supplied rectangular plate. The in-plane normal direction becomes the long transverse (T) direction, and the thickness, or through-ply direction is designated short transverse (S). The complete description of the fracture orientation requires assignment of a loading direction followed by crack advance direction. These two indicators are separated by a dash (–) to distinguish from the common designation for planes (e.g. L–T versus LT) [4, 5]. Specimens were prepared in the L–T, T–L, L–S, and T–S orientations for the discontinuous fibre material (Fig. 4). Owing to the limited quantities of continuous fibre material available for testing, specimens were prepared only in the L–T and L–S orientations.

2.4. Apparatus

All fracture tests were performed on a screw-driven load frame (Instron Model 4505) with a 100 kN load capacity, at a crosshead speed of 0.05 mm min^{-1}. The load–displacement (P–u) data were acquired by two independent methods. Hardcopies of load–displacement information were provided by a high-speed x–y chart recorder, and secondly, a direct computer link via a data acquisition board avoided manual manipulation. The three-point bend loading fixtures were manufactured from α-SiC. The punch was made from a 25 mm diameter solid SiC rod, and the lower fixtures were made from cylindrical SiC tubes with 6.3 mm wall thickness.

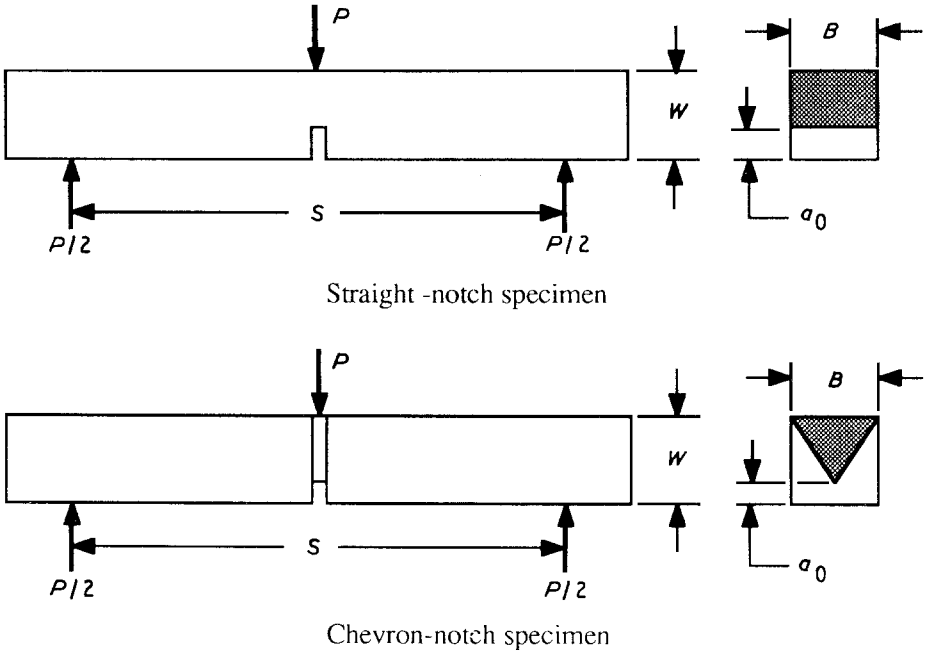

Figure 3 Schematic illustration of straight-notch and chevron-notch geometries.

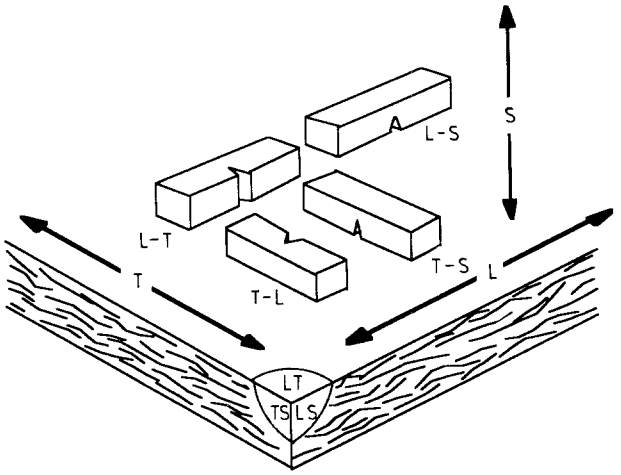

Figure 4 Schematic illustration of specimen orientations for the discontinuous fibre two-dimensional composite.

A custom-built vertical clamshell test furnace (Deltech Model DT-28-VT-SS) was used for all elevated temperature testing, where a positive pressure of argon maintained within the furnace minimized oxidation of the carbon specimens. Total specimen weight loss by oxidation was determined to be about 5% at 1400 °C. Those critical regions of the specimen deliberately protected by the argon stream, however, suffered considerably lower oxidation rates. Detailed SEM studies of the fracture surfaces revealed no evidence of decomposition at depths greater than about 100 μm from exposed edges of the crack.

2.5. Data reduction technique

The effective crack length is obtained by the compliance calibration technique, which requires the use of both the load–displacement data and the predetermined compliance calibration curve. The load-point-displacement (LPD) is obtained by subtracting the machine compliance from the experimentally observed compliances. Both the compliance calibration curve and the geometry correction factor are obtained from a modification of the numerical solutions of Jenkins *et al.* [6]. Fig. 5 schematically illustrates the data reduction technique. An experimentally determined factor, δ accommodates the large matrix damage zone inherent to these nonlinear composites [5]. The fracture surface energy, G_R, can be readily calculated from the relationship

$$G_{Ri} = \frac{\Delta U_i}{\Delta A_i} \quad (1)$$

where ΔU_i is the instantaneous fracture energy, evaluated from the area under the load–displacement curve for the ith increment of crack growth. The incremental crack surface area, ΔA_i, is determined from the effective crack length and the appropriate specimen dimensions.

The fracture toughness, K_{IC}, is evaluated at critical conditions by the relationship [7]

$$K_{IC} = \left(\frac{P_{max}}{BW^{1/2}}\right) Y \quad (2)$$

where P_{max} is the maximum load, B is the specimen thickness, W is the specimen width, and Y is the corresponding appropriate geometry correction factor.

2.6. Evidence of wake zone toughening mechanisms

The renotch procedure involves the mechanical removal of the wake region following the main crack tip, after a predetermined amount of stable crack growth. The fracture test is then continued after the renotching operation. Thus, the R-curve behaviour of the material can be evaluated in both conditions, with and without the presence of the following wake region.

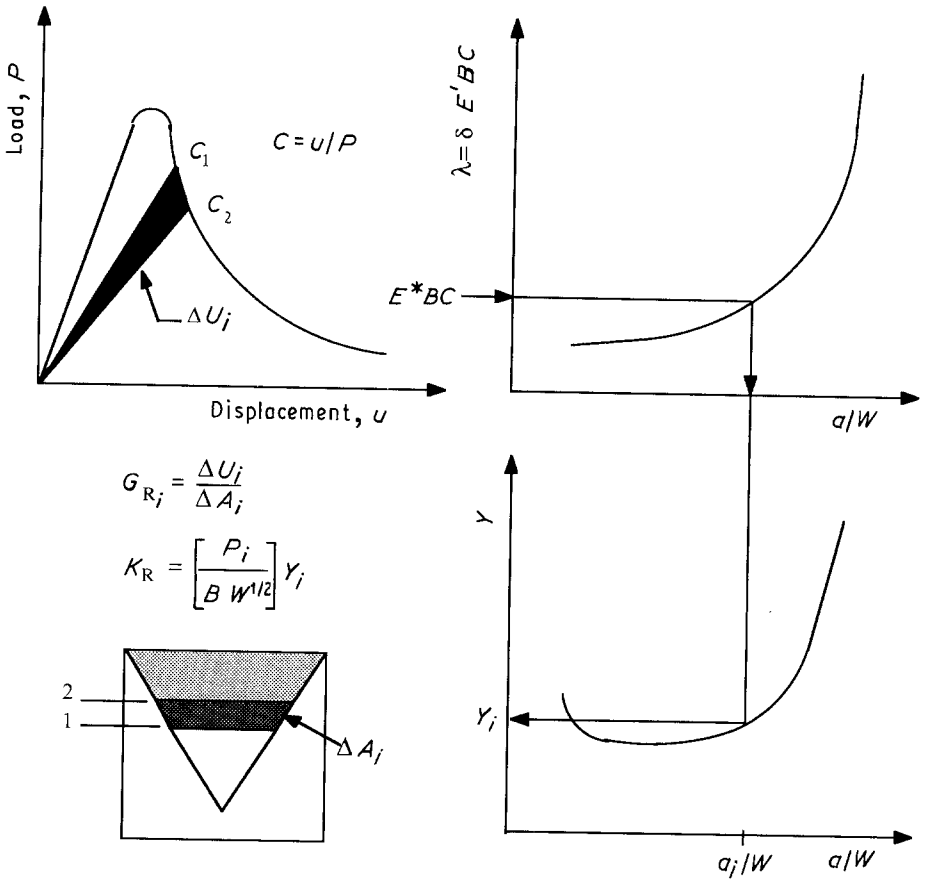

Figure 5 Data reduction method.

This technique was adopted from Knehans *et al.* [8], who proved the significance of the microstructural features in the following wake region in promoting the rising R-curve behaviour observed in coarse-grained monolithic alumina. More recent renotching studies conducted on monolithic alumina [9], as well as on a continuous SiC fibre-reinforced SiC-matrix composite [10], have proven the renotch test to be a useful tool for quantitatively separating the toughening contributions of the wake region from those of the frontal process zone. Essentially all rising R-curve behaviour displayed by these materials has been attributed to mechanisms operating in the wake.

A second evaluation of the effectiveness of the wake is obtained from a comparison of the K_{IC} values obtained with straight-notch and chevron-notch specimens. The wake development during subcritical crack growth in a chevron-notch specimen supports a significant portion of the applied load at critical conditions, where K_{IC} is measured [9]. This component of the microstructure is less available to participate in the fracture event at the machined notch tip of a straight-notch specimen. Therefore, an increased chevron-notch K_{IC} value in a rising R-curve material results directly from the toughening mechanism(s) operating behind the crack tip [5].

3. Results and discussion

Unlike many monolithic ceramics and carbons, both of the carbon/carbon composites included in this study display extremely stable fracture behaviour, regardless of specimen notch configuration. The straight-notch specimens in the L–S and T–S orientations tended to crack interlaminarly, perpendicular to the intended crack path. For this reason, G_R-curves and K_{IC} values were only reported for the chevron-notch configuration. The deep side slots of this notch orientation serve to constrain the crack to the plane of the macroflaw. Large-scale interlaminar cracking was not significant in any L–T or T–L specimen, with either style of notch, permitting the determination of both R-curves and critical stress intensity factors.

3.1. Load–displacement curves

Typical load–displacement records for L–T and L–S orientation chevron-notch fracture tests for both materials are presented in Fig. 6. These curves also characterize the material response in the T–L and T–S orientations, respectively. The curve shapes are nominally unchanged over the test temperature range, up to 1650 °C. While variations in specimen geometry influence load values somewhat, these variations are small enough to justify the following observations and interpretations of the relative values and shapes of the curves.

The continuous fibre woven composite sustains a maximum load that is twice that encountered by the felt-reinforced composite. The long fibre woven architecture is expected to enhance the load distribution throughout the matrix. Therefore, a larger volume of the specimen supports the applied load, which, in part, contributes toward the higher elastic stiffness and

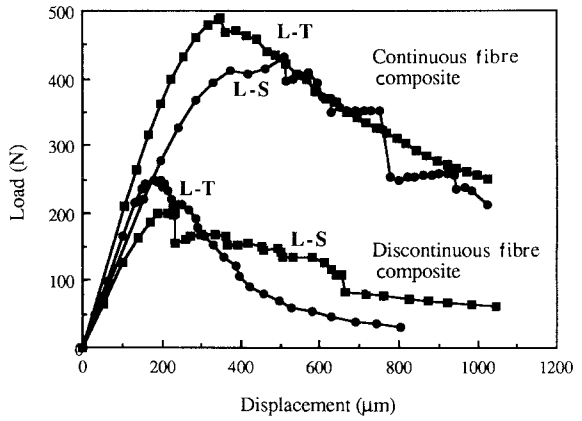

Figure 6 Load–displacement curves for chevron-notched specimens of both carbon/carbon composites tested at room temperature.

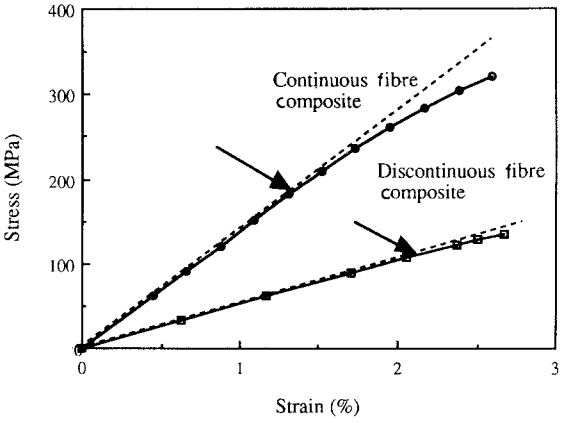

Figure 7 Stress–strain curves for thin L–T beams of both composites at room temperature. Arrows indicate proportional limits.

load-carrying capacity, P_{max}, over those of the discontinuous fibre composite.

The L–T curves of both materials indicate improved load-carrying properties when the crack propagates through all layers at once (T-direction), over the through-thickness direction (S-direction). This is also evinced by the relatively smooth L–T curves of Fig. 6. By comparison, the L–S curves are characterized by frequent load drops, corresponding to run–arrest crack propagation, which is also consistent with the stepped fracture surface appearance (to be addressed with reference to Figs 17 and 18). These precipitous load drops are probably associated with the failure of massive fibre groups as the crack progresses through the thickness of this layered structure.

The nonlinear behaviour observed prior to P_{max} for the L–S orientation of the discontinuous fibre composite, and to a larger extent for the L–T and L–S orientations of the continuous fibre composite, results in an increase in the effective subcritical crack growth. This phenomenon, in the present case attributed to long-range matrix damage, is examined through the stress–strain curves of Fig. 7. The difference in proportional limits indicated on the figure, is invariant with the more extensive matrix cracking observed in the continuous fibre composite, presumably resulting from the characteristic long-range load distribution of this fibre architecture. The ultimate strengths differ by about a factor of 2.5, however, the proportional limit of the continuous fibre composite is only about 60% higher than the felt-reinforced material. The proportional limit of the continuous fibre composite is only 58% of ultimate stress, compared with almost 90% for the short fibre architecture. Because this difference in matrix contribution suggests a more prominent role of the longer fibres, even after extensive matrix damage, it must also be inferred that the volume of material included in the damage zone is directly related to the fibre length.

3.2. Crack growth resistance curves

Crack growth resistance curves corresponding to the room temperature L–T and L–S chevron-notch load–displacement curves of Fig. 6, are shown in Fig. 8, in terms of the fracture surface energy term, G_R. The

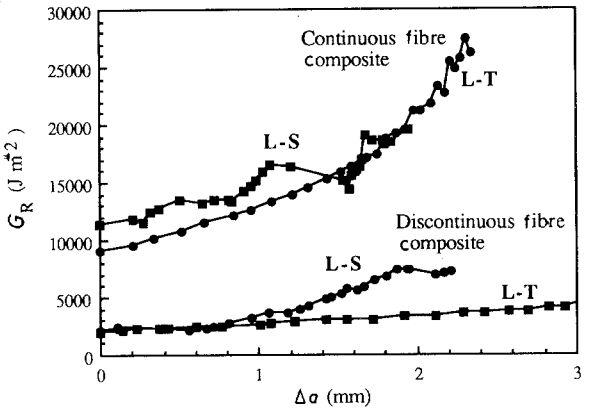

Figure 8 G_R-curves for L–T and L–S orientation chevron-notched fracture experiments of both composites at room temperature.

higher value of G_{IC}, by about a half order of magnitude, and the improved slopes, both characterize the stronger crack growth resistance of the continuous fibre composite. Again, this difference in magnitude is attributed to the differing fibre architectures, where the higher values of $dG_R/d\Delta a$ for the continuous fibre composite, represents a heightened effectiveness of the mechanisms responsible for cumulative toughening behaviour. This implies that a more extensive fracture process zone associated with the long fibre structure, provides more efficient crack tip shielding.

The long fibre cumulative mechanism appears earlier in the fracture event. The pronounced R-curve rise of the continuous fibre materials immediately follows critical conditions, while the comparable test for the felt architecture requires about 0.8 mm crack growth to develop a comparable slope. The slope of the long-fibre L–T experiment finds no competition, even at very large crack lengths.

The run–arrest character determined for cracks travelling in the through-ply direction for both of these architectures, typifies all layered structures [11–13], where interlaminar damage and crack arrest at successive layers promotes the characteristic run-arrest behaviour observed for the present composites. While little difference in average $dG_R/d\Delta a$ appears between the two continuous woven orientations, an

obvious advantage in cumulative toughening appears for the L–S short fibre results.

3.3. High-temperature behaviour

The G_R-curve behaviour for the L–T orientation specimens of the Kobe material, shown in Fig. 9, remains unchanged up to 1050 °C, then, after a significant decrease in both slope and G_{IC} at 1400 °C, it exhibits very high crack growth resistance at 1500 and 1650 °C. This behaviour is generally consistent with the reported strength increase at elevated temperatures, unique to carbon materials [1]. However, the decrease in 1400 °C fracture properties is singular to this discontinuous fibre composite. Preliminary microstructural results which follow, suggest that the observed fracture behaviour at 1400 °C is attributable to the development of a fibre/matrix interfacial reaction zone appearing near 1400 °C and becoming more pronounced with increasing temperature. A transition in the organization of this critical zone would undoubtedly be accompanied by a change in the fibre/matrix interfacial properties.

Crack growth resistance curves for the L–T orientation of the ACC-4, at four test temperatures up to 1650 °C are shown in Fig. 10. Room temperature to 1400 °C provokes very little change over this broad test-temperature range, with $dG_R/d\Delta a$ nearly identical over more than 2 mm crack growth. At yet higher temperatures, the R-curve slope is maintained, although at a much higher level of resistance.

The greater G_{IC} values measured for both composites, indicates an enhanced resistance to crack initiation at 1650 °C, which is independent of fibre architecture. However, because only a minor slope increase is consistently evident, this improvement must be restricted to those microstructural changes which influence toughness through largely non cumulative contributions. The two elements considered most likely to contribute in this way include the inherent strength increase of carbon at higher temperatures, and the temperature-dependent characteristics of the fibre/matrix interface. Both could conceivably delay initiation to higher applied loads,

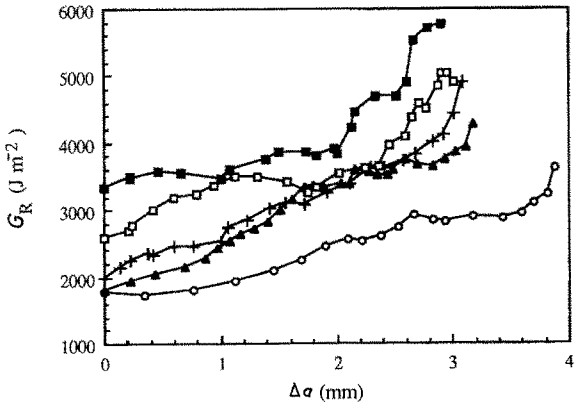

Figure 9 G_R-curves for L–T chevron-notched fracture experiments of discontinuous fibre carbon/carbon composite at temperatures up to 1650 °C. (+) 20 °C, (▲) 1050 °C, (○) 1400 °C, (□) 1500 °C, (■) 1650 °C.

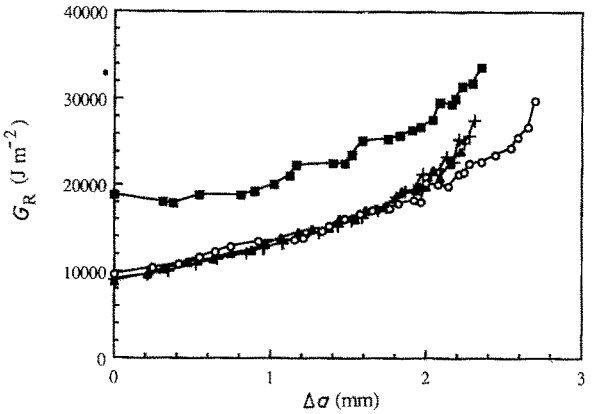

Figure 10 G_R-curves for L–T chevron-notched fracture experiments of continuous fibre carbon/carbon composite at temperatures up to 1650 °C. (+) 20 °C, (▲) 1200 °C, (○) 1400 °C, (■) 1650 °C.

without affecting the cumulative component; however, the most ostensible scenario would include multiple, competitive events.

3.4. Renotch tests

Although the existence of rising R-curves indicates the presence of a cumulative toughening mechanism in the material, no distinction between influences from the frontal process zone or from the wake region can be deduced from this information alone. The renotch test provides a quantitative evaluation of the toughening contribution from the following wake region in these rising R-curve materials. The load–displacement records for chevron-notch, L–T orientation renotching experiments performed at room temperature are presented in Figs 11 and 12, for the discontinuous and continuous fibre composites, respectively. Initial loading proceeds through P_{max} at point A, to point B where the test is interrupted for the renotching procedure. Note that upon unloading, closure effects are evinced by the displacement offset to point C. After renotching, the specimen is reloaded from point C through point D to completion of the test. These data clearly illustrate the dramatic role of the following wake region in both of these composites, with no fracture mechanics assumptions required. Removal of the wake zone by renotching reduces the load required for continued extension of the crack from the final load of the initial curve, by about 35% for the discontinuous fibre composite, and by almost 50% for the continuous fibre composite. Furthermore, the compliance increase after removal of the wake zone clearly supports the dominant role of the following wake zone load carrying capacity in this sharp-cracked specimen.

The reduced load–displacement data are presented as crack growth resistance curves in Figs 13 and 14. The point of maximum load, A, is used for the calculation of K_{IC} and also serves as the initial point of the R-curve analysis. During initial loading of this chevron-notch specimen, the crack propagated sub-critically from $a_0/W = 0.50$ to $a_0/W = 0.63$. This allows 1.3 mm crack length for the development of a wake region when critical conditions are reached for the

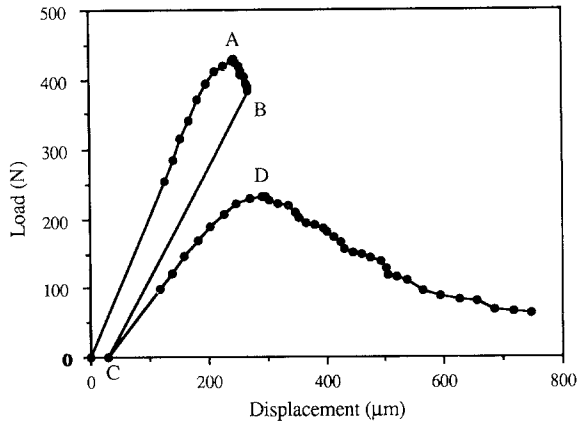

Figure 11 Load–displacement curves of a renotch test on a chevron-notched discontinuous fibre carbon/carbon composite specimen at room temperature.

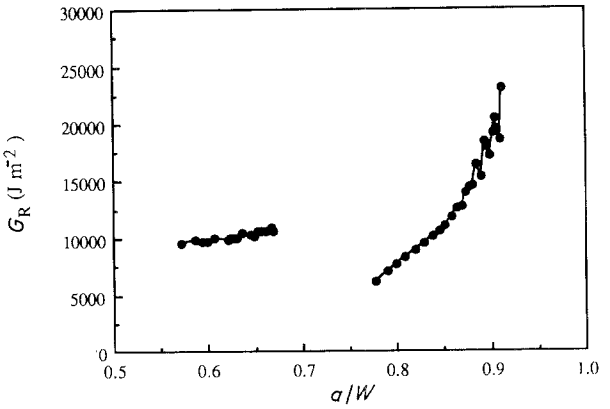

Figure 14 G_R-curves of a renotch test on a chevron-notched continuous fibre carbon/carbon composite specimen at room temperature.

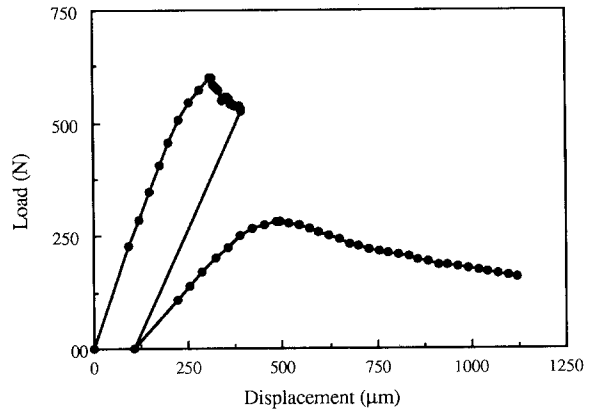

Figure 12 Load–displacement curves of a renotch test of a chevron-notched continuous fibre carbon/carbon composite specimen at room temperature.

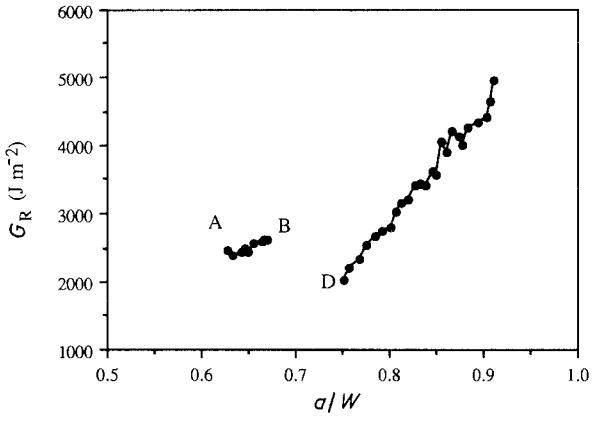

Figure 13 G_R-curves of a renotch test on a chevron-notched discontinuous fibre carbon/carbon composite specimen at room temperature.

determination of K_{IC} and G_{IC}. The relatively large amount of subcritical crack growth in this composite compared with many brittle materials [9] provides additional evidence of its highly stable fracture behaviour, as established earlier for the load–displacement curves in Fig. 6 and the G_R-curves in Fig. 8. For the Kobe material, the fracture surface energy increases from 2450 J m^{-2} to 2620 J m^{-2} prior to renotching. After wake removal, the G_R value drops to 2015 J m^{-2}, as a direct result of the elimination of those microstructural features behind the primary crack tip which contribute toward cumulative toughening. As the crack progresses, the instantaneous G_R values again rise strongly, with continued wake zone development.

The lower critical G_R value after renotching, below G_{IC}, may be explained by the following factors. A larger load is required to initiate a crack from a renotched specimen, as it attains critical conditions in a configuration which closely approaches that of a straight-notch specimen [9]. Probably of greater significance, however, is the proportionally smaller wake region which results from the reduced subcritical crack extension following renotching, compared with that observed initially, at P_{max}.

In the case of the ACC-4, removal of the wake zone by renotching reduces the load required for crack reinitiation by 45% from the final load on the initial curve. Also, the compliance of the linear portion of the reloading curve increases significantly from the unloading curve. The fracture surface energy increases from 9600 J m^{-2} to 10900 J m^{-2} prior to renotching. After renotching, a decrease to 6100 J m^{-2}, is followed by a strong increase with continued crack growth as a new wake develops. These renotch tests appropriately formalize the toughening contribution from the wake region, throughout the test-temperature range. Extensive fibre pull-out and fibre bridging, produces frictional energy dissipation at the fibre–matrix interface, and lowers the effective crack tip stress by supporting a significant portion of the total load.

Fig. 15 illustrates the effect of test temperature on the drop in fracture surface energy, ΔG_R, after renotching, for the L–S and L–T orientations of both materials. While ΔG_R, an indicator of the wake zone "effectiveness", decreases consistently for both orientations in the discontinuous fibre composite, a significant rise is apparent for the continuous fibre composite. This suggests that the sliding–debonding phenomenon characteristic of fibre pull-out is strongly controlled by a temperature-dependent fibre/matrix interface structure which exists only in the woven

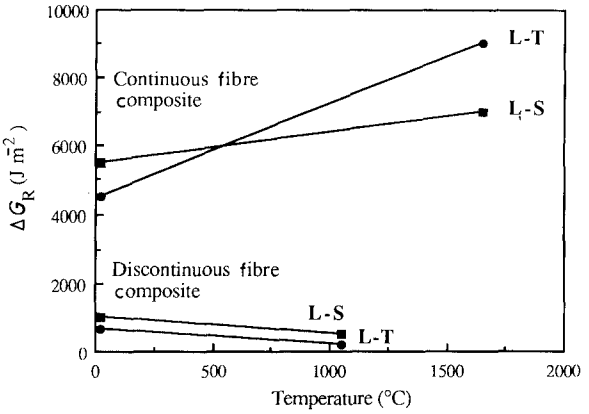

Figure 15 Drop in fracture surface energy during renotch tests on L–T and L–S chevron-notched specimens for both carbon/carbon composites at temperatures up to 1650 °C.

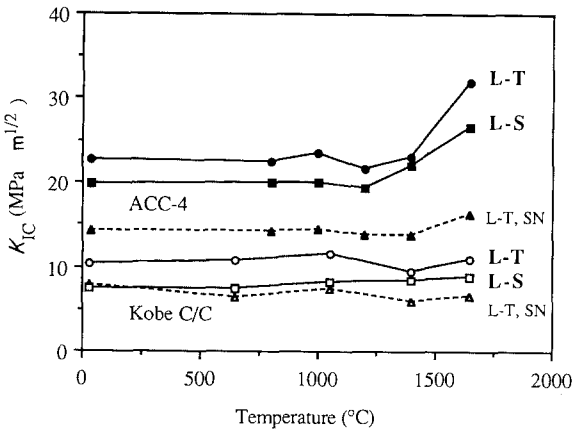

Figure 16 Fracture toughness versus temperature for L–T and L–S chevron-notched and L–T straight-notched specimens for both carbon/carbon composites. ACC4, continuous fibre composite; Kobe, discontinuous fibre composite. (●) ACC4 L–T chevron-notched, (■) ACC4 L–S chevron-notched, (▲) ACC4 L–T straight notched, (○) Kobe L–T chevron-notched, (□) Kobe L–S chevron-notched, (△) Kobe L–T straight notched.

composite over the temperature range of these experiments. Additional testing is required to evaluate the temperature range above 1400 °C in the Kobe material.

The ΔG_R relationship between the two materials is in close agreement with the uninterupted *R*-curves of Fig. 8. The ACC-4*R*-curve behaviour is, in both level and slope, between one-half and one order of magnitude above that of the felt composite. Comparing the G_R-curve slopes, at about 1.3 mm crack extension for consistency, the renotch results also fall within this range.

3.5. LEFM fracture toughness

Fig. 16 compares the fracture toughness of both materials, throughout this test-temperature range, for both notch types and orientations (straight-notch L–S omitted). For the discontinuous fibre material, the chevron-notch K_{IC} values increase slightly with test temperature, compared with a nearly constant fracture toughness for the continuous fibre architecture. While, the G_R-curves appear to be equivalent for the L–T and T–L orientations, the higher K_{IC} values for both notch configurations of the L–T orientation specimens are explained by the porosity distribution which has been previously reported [5].

The 60% greater K_{IC} values for the L–T chevron-notch specimens compared with the corresponding straight-notch values, result directly from the toughening contribution from the fibre bridging and pull-out mechanisms in the following wake region. Similarly, the stronger chevron-notch fracture toughness at 1650 °C is directly related to the enhanced high-temperature *R*-curve behaviour shown in Fig. 10. Comparable to the renotched specimens, the increased wake region contribution characteristic of the chevron-notch geometry, is considerably less pronounced at the machined notch tip of straight-notch specimens [9]. Further supporting this view, the fracture toughness values obtained from the discontinuous fibre composite shows only about 30% difference between the two notch types, which agrees with the more modest *R*-curve behaviour, already aired for this material. The woven, continuous fibre architecture provides the more fracture resistant composite, as evinced by the consistent factor of two difference in toughness between the two materials (Fig. 16). Secondly, the higher total porosity of the discontinuous fibre composite has been shown to decrease toughness in other fibre-reinforced composite materials [5].

3.6. Microstructural analysis

Low-magnification scanning electron micrographs of L–S fracture faces are shown in Figs 17 and 18 for chevron-notch specimens of both composites. By comparison, the L–T orientation fracture faces are relatively flat, with no major deviations in crack path. Pull-out lengths of 1 mm or less are typically for the discontinuous fibre composite, and 1–2 mm for the continuous fibre composite. On the other hand, L–S orientation fracture faces display fibre pull-out lengths of up to 2 mm for the discontinuous fibre composite, and up to 6 mm for the continuous fibre composite. The overall ledge-like appearance, as the crack meanders on short interlaminar excursions, is believed to contribute to the relatively high fracture surface energies and strongly rising *R*-curves, characteristic of the L–S orientation [5]. The delamination toughening component, typical of this specimen orientation, enlarges the fracture process zone and results in a greater measured fracture surface energy [10, 14].

The longer pull-out length found in the continuous fibre material is expected to permit the development of a significantly longer wake zone behind the primary crack tip. However, the absence of a plateau in the rising *R*-curves for both materials precludes a direct evaluation of this, as the wake length apparently exceeds the specimen width, *W*, for both materials. Despite earlier studies which suggest a uniform distribution of traction stresses throughout its length, independent of COD [15, 16], the effectiveness of the wake zone for the present composites is expected to be strongly influenced by the volume of damaged material associated with the process zone. Longer fibre pull-

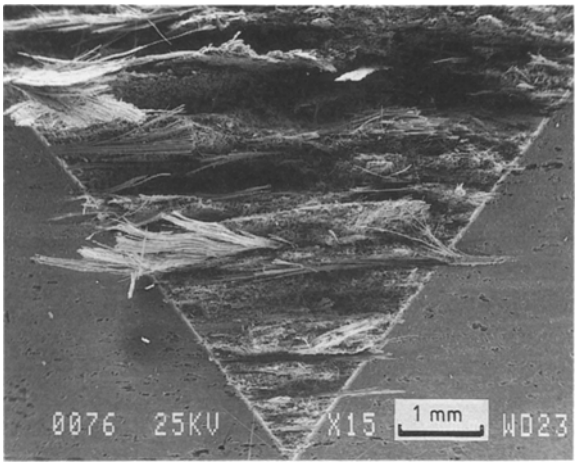

Figure 17 Scanning electron micrograph of an LS fracture surface of a discontinuous fibre composite chevron-notched specimen tested at 20 °C.

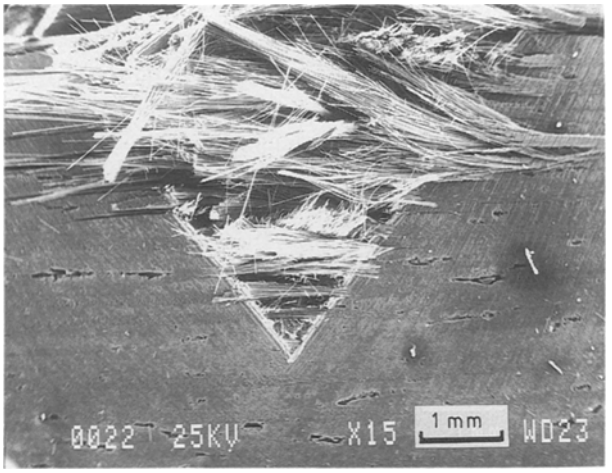

Figure 18 Scanning electron micrograph of an LS fracture surface of a continuous fibre composite chevron-notched specimen tested at 20 °C.

out lengths may increase this volume by involving more material in the fracture event. Although the metal/polymer experiments of Cook *et al.* [16] have determined a scarce dependence of embedded fibre length on the frictional interfacial shear stress, the failure of fibres at distant locations within the wake zone and the damage accumulation in the adjacent volume of matrix material participating in the pull-out process, are expected to require additional fracture energy for crack extension. So the nature of matrix separation from the fibre will influence the damage zone extent, beyond simply the pull-out from a sheath, as was represented by the Cook data.

Based upon test results of Figs 6 and 7, extensive subcritical matrix damage is advanced to account for the significantly higher loads supported by the continuous fibre architecture. Although both architectures use the same PAN-based T-300 fibre, the observed pull-out length for the continuous fibre composite is consistently two to three times larger than for the felt-reinforced material. Because the shortest as-processed fibre exceeds these lengths by more than one order of magnitude, apparently the intrabundle matrix interface controls the balance between pull-out and fibre breakage. The lower fracture surface energy associated with the felt-reinforced material is, therefore, more related to the modest fibre pull-out, associated with the characteristic debonding/pull-out character described below.

Fig. 19 shows a protruding bundle of fractured fibres typical of the discontinuous fibre composite. It denotes the tendency of this material to debond by groups of 10–30 aligned fibres. As the matrix material appears undamaged within each bundle, no intrabundle microcracking nor debonding occurs during the fracture event. Because of the significant fibre-to-fibre bonding which is apparent within the bundles of this composite, a bundle will fracture at the largest local defect along the loaded bundle length [5]. The fibre/intrabundle matrix interfacial strength, then, appears to be too high to permit individual fibre pull-out within bundles. The interbundle matrix, typically approximated by the second infiltration step (pitch), seems to provide the primary deformation path for composite failure. This character dramatically reduces that portion of the material potentially available for fibre debonding, and therefore diminishes the corresponding fracture energy.

The continuous fibre composite displays significantly larger fibre bundle pull-out lengths, as shown in Fig. 20. It is readily apparent that these sizeable pull-out lengths easily provide fibre bridging through the maximum crack opening displacement of 150–180 μm typical for this composite. This extensive fibre pull-out is believed to be responsible for the high fracture surface energies and strongly rising *R*-curves characteristic of both the L–T and L–S specimen orientations. Also, an extensive matrix damage zone contributes to the composite toughness, because the woven fibre architecture experiences composite strains which far exceed the elastic limits of the brittle matrix material [17].

The continuous fibre composite utilizes only a resin matrix precursor, rather than the resin and pitch precursors employed in the production of the discontinuous fibre/hybrid matrix composite [2]. The

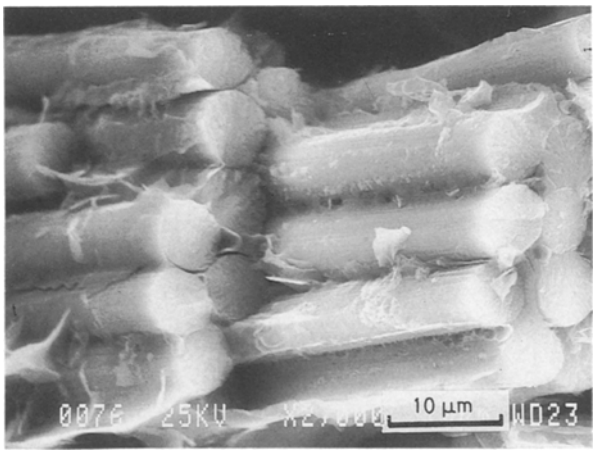

Figure 19 High-magnification scanning electron micrograph of an LS fracture surface of a discontinuous fibre composite chevron-notched specimen tested at 20 °C.

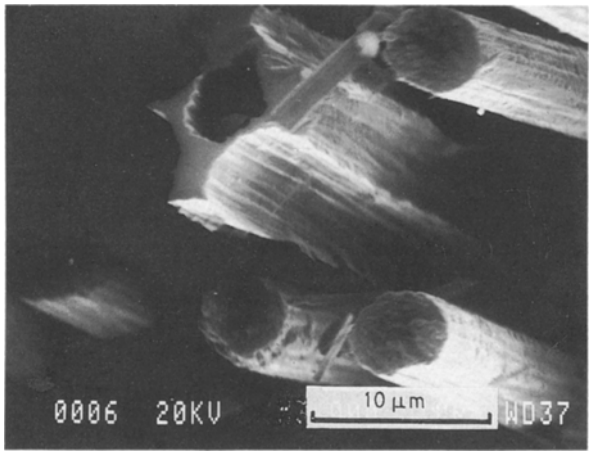

Figure 20 High-magnification scanning electron micrograph of an LS fracture surface of a continuous fibre composite chevron-notched specimen tested at 20 °C.

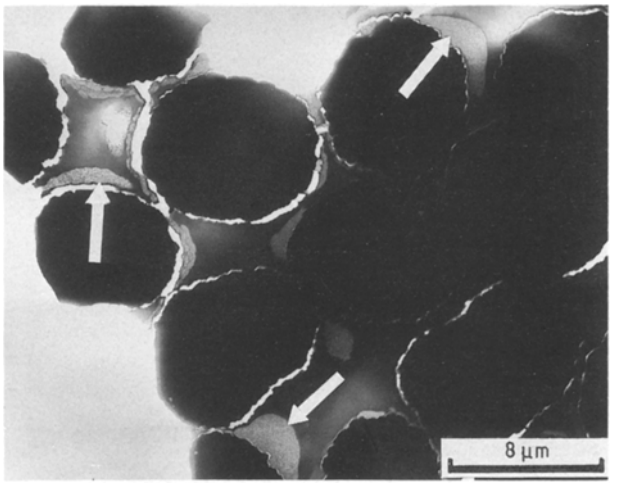

Figure 21 Bright-field transmission electron micrograph of a transverse cross-section of a continuous fibre composite tested at room temperature showing the fibre/matrix interphase zone (arrowed).

continuous fibres do not appear to be chemically bonded to one another, but are rather surrounded and joined by matrix material. This is strongly contrasted with the intimately attached fibre bundles of the felt composite, as discussed above. The predominantly mechanical fibre–matrix interfacial bond results in a low interfacial bond strength [11, 17], and facilitates the fibre pull-out mechanism responsible for most of the observed toughening behaviour of this composite.

Transmission electron microscopy has revealed an irregularly distributed "reaction zone" at the fibre matrix interface of the continuous fibre composite. This phase, found in specimens tested at all temperatures, is presumed to result from the fabrication process rather than the test environment. The bright-field micrograph of Fig. 21 and the diffraction patterns of Fig. 22 indicate the lower order of crystallinity of the fibre/matrix interphase compared to that of the carbon matrix. This distinct interphase structure exhibits a preferred orientation with respect to the matrix. Although the details are the subject of further study, the thermal expansion mismatch resulting from this crystallographic relationship across the interface is believed to influence debonding and sliding at the higher temperatures.

A similar interphase has been identified in the discontinuous fibre composite, however, primarily in samples subjected to test temperatures of 1400 °C and above. As previously noted, the appearance of this fibre/matrix reaction zone coincides with, and may contribute towards, the sharp decrease of fracture properties at 1400 °C. The early developmental stages of this reaction zone apparently provide inappropriate fibre/intrabundle interfacial characteristics, which adversely affect the fracture properties. The corresponding effect on fibre pull-out efficiency may result from local thermal expansion mismatch arising from crystallographic orientational effects. Moreover, considering the extent of chemical bonding between the matrix and the fibre, it is also suggested that carbonization of the interfacial chemical groups may lead to this transitional impairment of pull-out. However, the structural similarity with the interphase found in the continuous fibre composite, which is apparently independent of test temperature, supports the improved fracture behaviour observed at 1500 and 1650 °C.

If this interphase is assumed to be of a lower strength than the matrix material, then the enhancement of the mechanism of individual fibre debonding is supported. This interphase would therefore contribute to the high fracture surface energy involved in the failure of the continuous fibre material throughout the test-temperature range, and of the felt-reinforced composite above 1400 °C. Although the exact structure of this interphase and its temperature dependence are still under study, its mechanical properties apparently play a key role in the micromechanisms involved in the high-temperature fracture properties of these composites.

3.7. Summary of results

The mechanisms controlling fracture of the two carbon/carbon composites may be inferred from the multiple sources of evidence provided by this study. Considering the fracture process by its constituents, the total observed crack growth resistance, G_R, is composed of the cumulative and non cumulative components, ΔG and G_i, respectively. At any point along the R-curve, both of these elements may be of significance, however, the initiation quantity, G_i, uniquely influences the growth from a critical flaw under no influence from a process zone. Although in practice this is difficult to isolate, the initiation from a straight-notch specimen closely approximates this condition. By contrast, the chevron-notch becomes unstable at a crack length beyond the machined surfaces, forcing the heightened cumulative influence discussed above. Each subsequent point along the G_R-curves represent both cumulative and non cumulative contributions, while the slopes of these curves are influenced only by the cumulative components. Furthermore, because the straight-notch critical stress intensity factor data suppress the cumulative effects, this quantity may be subtracted from the chevron-notch results to isolate

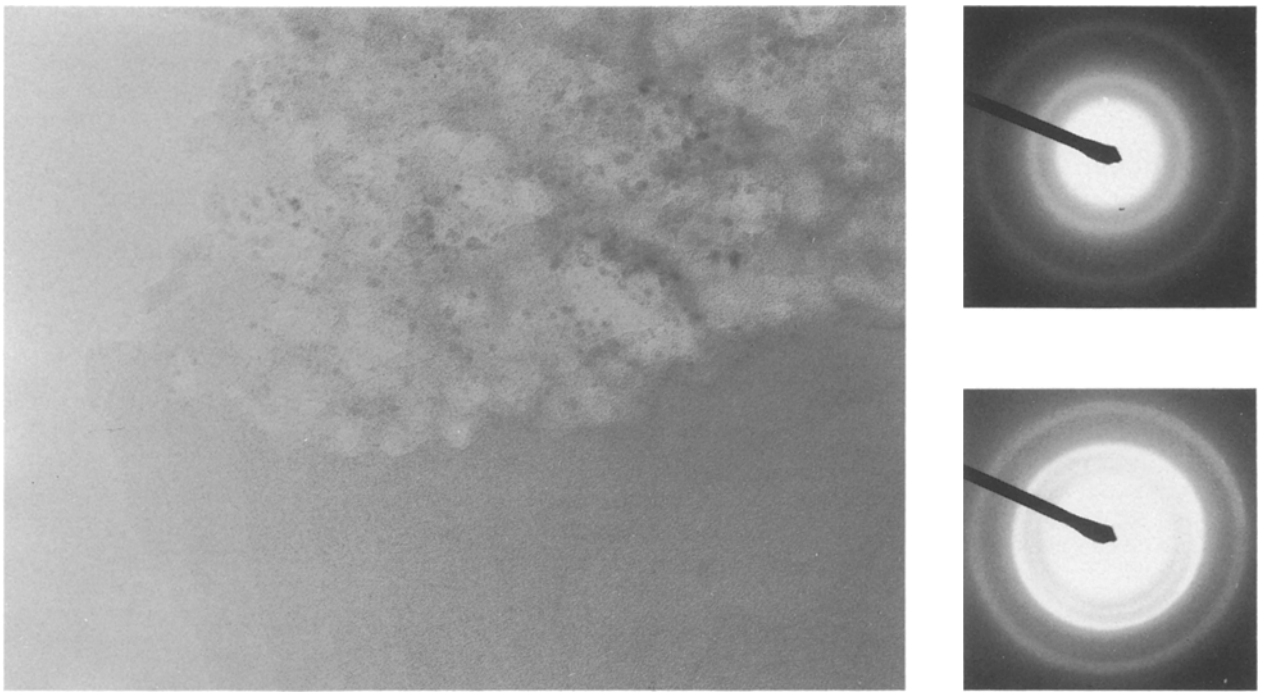

Figure 22 Bright-field transmission electron micrograph of the interface between the interphase layer and the carbon matrix and associated diffraction patterns for the continuous fibre carbon/carbon composite.

the ΔG component at that crack length. This quantity, ΔK_{IC}, represented by the difference between chevron- and straight-notch fracture toughness results found in Fig. 16, principally compares with the renotch results, ΔK_R, which is an independent measure of the wake component of the cumulative toughening, although at an advanced crack length.

The elements which contribute towards fibre bridging behind the primary crack tip include the strength of the fibre and of the matrix and the character of the interface. The non cumulative elements resist crack extension through the front-field microstructure. This includes crack deflection, strength, and the inherent ability of the composite to blunt the crack tip through damage zone development. The data presented in this study support contributions from virtually all of the above mechanisms; however, the role of fibre bridging clearly dominates the toughening behaviour of both composites, and underlines improved performance of the continuous, woven architecture of the ACC-4.

At room temperature the ACC-4 demonstrates the superior G_i and ΔG, as both K_{IC} and $dG_R/d\Delta a$ significantly exceed those of the Kobe composite. The larger cumulative wake component of the ACC-4 is evident in the greater ΔK_{IC} and ΔK_R quantity. At elevated temperature, these quantities separate even further, with the ACC-4 improving considerably. The strength of the carbon structures and the interfacial character, identified above, are advanced as the primary microstructural contributions toward these phenomena, at both ambient and elevated temperatures.

4. Conclusions

The fracture behaviour of two carbon/carbon composite materials has been characterized over the range of test temperatures from 20–1650 °C. Complete crack growth resistance curves displayed rising R-curve behaviour for all temperatures throughout this range. Although, the toughness and R-curve behaviour of the discontinuous fibre composite improved with increasing test temperature, up to 1650 °C, these properties of the L–T test orientations suffer a marked decrease at 1400 °C. This behaviour is contrasted with the orderly increase in crack growth resistance with increasing temperature throughout this range, which characterizes the continuous fibre composite.

This temperature dependence of the fracture processes may be influenced by two microstructural changes. The natural strengthening of carbon materials with increasing temperatures undoubtedly contributes toward the observed behaviour. However, the role of the matrix/reinforcement interface is evident from the tendency of the discontinuous fibre composite to fail by large groups of aligned fibres rather than individually. A structural transformation of this interface region, through the appearance of an interfacial reaction zone is advanced to explain the 1400 °C transition in fracture properties.

The dominant role of the pull-out mechanism in the following wake region has been confirmed through the following two approaches. Renotching experiments indicate a finite wake zone contribution at all test temperatures, for both composites. This character, quantified by ΔG_R, is shown to slightly decrease with test temperature for the discontinuous fibre composite, while the continuous fibre composite improves by 10%–50%. A second indicator of wake zone toughening effectiveness may be obtained from the high-temperature behaviour of the chevron-notched K_{IC}, compared with that derived from the straight-notch type. Above 1400 °C, the wake zone component of the

chevron-notch fracture toughness increases significantly, while the values acquired from straight-notch specimens change litttle.

References

1. S. AWASTHI and J. L. WOOD, *Ceram. Eng. Sci. Proc.* **9** (1988) 553.
2. D. HUNN and R. BELARDINELLI, in "Proceedings of Composites in Manufacturing 7", Long Beach, CA (1987).
3. M. F. KANNINEN and C. H. POPELAR, "Advanced Fracture Mechanics" (Oxford University Press, New York, 1985).
4. D. BROEK, "Elementary Engineering Fracture Mechanics" (Nijhoff, The Hague, 1984).
5. S. SENET, R. E. GRIMES, D. L. HUNN and K. W. WHITE, *Carbon* **29** (1991) 1039.
6. M. G. JENKINS, A. S. KOBAYASHI, K. W. WHITE and R. C. BRADT, *Int. J. Fract.* **34** (1987) 281.
7. D. MUNZ, *Engng Fract. Mech.* **15** (1981) 231.
8. R. KNEHANS and R. STEINBRECH, *J. Mater. Sci. Lett.* **1** (1982) 327.
9. R. E. GRIMES, G. P. KELKAR, L. GUAZZONE and K. W. WHITE, *J. Amer. Ceram. Soc.* **73** (1990) 1399.
10. K. W. WHITE, R. C. BRADT and A. C. KOBAYASHI, "The Effect of the Wake Region on the Fracture Behavior of SiC Reinforced Composites", 12th Conference on Composites, Materials, and Structures, Cocoa Beach, FL (1988).
11. E. FITZER, *Carbon* **25** (1987) 163.
12. S. OCHIAI and P. W. M. PETERS, *J. Mater. Sci.* **17** (1982) 417.
13. M. SAKAI, R. C. BRADT and D. B. FISCHBACH, *ibid.* **21** (1986) 1491.
14. F. K. KO, *Amer. Ceram. Soc. Bull.* **68** (1988) 553.
15. P. F. BECHER, C.-H. HSUEH, P. ANGELINI and T. N. TIEGS, *J. Amer. Ceram. Soc.* **71** (1988) 1050.
16. R. F. COOK, M. D. THOULESS, D. R. CLARKE and M. C. KROLL, *Scripta Metall.* 23 (1989) 1725.
17. L. E. JONES, P. A. THROWER and P. L. WALKER, *Carbon* **24** (1986) 51.

Received 9 November 1990
and accepted 10 April 1991